ACS APPLIED NANO MATERIALS

Strain Modulated Electronic, Mechanical and Optical Properties of the Monolayer PdS, PdSe, and PtSe for Tunable Devices

Shuo Deng, Lijie Li, and Yan Zhang

ACS Appl. Nano Mater., **Just Accepted Manuscript** • DOI: 10.1021/acsanm.8b00363 • Publication Date (Web): 13 Apr 2018

ACS Publications

is published by the American Chemical Society. 1155 Sixteenth Street N.W., Washington, DC 20036

Strain Modulated Electronic, Mechanical and Optical Properties of the Monolayer PdS_2, $PdSe_2$, and $PtSe_2$ for Tunable Devices

Shuo Deng[†‡], Lijie Li*[‡], Yan Zhang*[¶]

[†]School of Logistic Engineering, Wuhan University of Technology, Wuhan 430070, China
[‡]College of Engineering, Swansea University, Swansea, SA1 8EN, United Kingdom
[¶]School of Physics, School of Physical Electronics, University of Electronic Science and Technology, Chengdu 610054, China

Abstract

We study the electronic, mechanical and optical properties of the monolayer PdS_2, $PdSe_2$ and $PtSe_2$ under mechanical strains of various magnitudes and directions. It is found that the band structures of these materials are more sensitive to biaxial strains. Moreover, the Young's modulus of all three materials are calculated in the *a* and *b* directions. Simulation results show the Young's modulus of monolayer PdS_2, $PdSe_2$ and $PtSe_2$ are 116.4 GPa, 58.5 GPa and 115.9 GPa in the *a* direction and 166.5 GPa, 123.6 GPa and 117.7 GPa in the *b* direction. We analyze the peak shift of the real (ϵ_1) and imaginary (ϵ_2) parts of the complex dielectric constants for these three materials. We found that the peak of the complex dielectric constant red-shifts towards lower energy and $\epsilon_1(0)$ monotonously increase with the compressive and tensile strains increase. Among these three materials, PdS_2 exhibits excellent electronic and optical tunability under tensile strains, for example the peak wavelength of the imaginary dielectric constant can be adjusted from 2 eV to 1 eV when the strain varies from 0% to 10%, leading to approximately 5% red-shift in wavelength per 1% mechanical tensile strain. The results indicate that these monolayer materials will have potential applications in tunable nanoelectromechanical devices.

Key Words

Transition metal dichalcogenides materials, Electronic properties, Optical properties, Mechanical properties, Strain modulation, First principle simulation

1 Introduction

The traditional transition-metal dichalcogenides (TMDs) semiconductors have generated great research interests thank to their superior electronic, optical, mechanical and catalytic properties[1-9]. For example, they exhibit a direct bandgap between 1.1 eV and 2.0 eV at the *K* point[10-12], strong photoluminescence and piezoelectric effects[10, 13-15] and offer of full optical control of the valley and spin occupation[16-19]. These material properties will bring much benefit in applying them to many devices and systems such as strain sensors[20], high speed photodetection[21], and transistor device[22]. The traditional TMDs were extensively investigated both in theory and experiment in the past[3, 20, 23-26].

The pioneering studies demonstrated that traditional TMDs have been mainly focused on the semiconducting with each transition metal atom bind to six S or Se atoms[12]. Recently, it was theoretically and experimentally demonstrated that some noble metals can also form layered structures with S or Se atoms, such as PdS_2, $PdSe_2$ and $PtSe_2$[27-29]. In PdS_2 and $PdSe_2$, each Pd atom can bond to four S or Se atoms, respectively. In $PtSe_2$, the unit cell consists of one Pt and two Se atoms. These novel structures lead to the formation of some important properties distinguished from the traditional TMDs, such as more air stability, high electron mobility, enhanced thermoelectric properties, superconductivity and so on[28, 30-32]. Many previous studies have shown that it is one of effective ways to adjust the properties of TMDs using mechanical strains[12, 23-26]. A few research groups have heoretically demonstrated the electrical and optical properties of monolayer PdS_2, $PdSe_2$ and $PtSe_2$[33-38]. Although there have been tremendous theoretical efforts reported, there is a lack of a detailed analysis of full electrical, optical and mechanical properties change of monolayer PdS_2, $PdSe_2$ and $PtSe_2$ under strains in different magnitudes and directions. In our work, we found that the effect of biaxial strains on tunable electronic and optical properties of these materials are more

significant than uniaxial strains. Among these three monolayer materials, the monolayer PdS_2 exhibits excellent electronic and optical tunability under tensile strains.

The design of novel and high-performance devices requires a thorough understanding of underlying materials properties such as mechanical, electrical, and optical properties, which can be done through state-of-art first principles methods. We have used the first principles method to gain in-depth and full understanding of these three emerging monolayer materials in terms of their mechanical, electronic and optical properties, from which some new results have been obtained and presented in the manuscript. In this paper, we simulate the electronic, mechanical and optical properties of monolayer PdS_2, $PdSe_2$ and $PtSe_2$ under a deformation range from -10% (compressive strain) to +10% (tensile strain) with variations in direction and magnitude using the first-principles method. This method has been applied in previous studies on many traditional TMDs[23-26]. Our target is to theoretically investigate the change of band structures, Young's modulus, and the complex dielectric constant under different strains. Section 2 describes the modelling and computational method in our simulations, section 3 details the simulation results and theoretical analysis of the electronic, mechanical and optical proprieties under different strains.

2 Simulation procedure

Three monolayer materials named as PdS_2, $PdSe_2$ and $PtSe_2$ have been investigated using the Atomistix ToolKit (ATK)[39]. For convenience, we refer to these materials as the TW_2 (*T*, transition-metal atom; *W*, chalcogen atom) type. Then, the lattice constants and key bond angles/lengths are shown in the Table S1 (in the Supporting Information). In the Figure 1, the TW_2 are composed by stacking of two-dimensional (2D) *W-T-W* sheets. The unit cells (red solid line) are indicated in the Figure 1. Although, there are several possible geometries (arrangements of atoms) for PdS_2, $PdSe_2$, and $PtSe_2$ 2D materials. First, we simulated similar geometries for these three materials for the purpose of comparison. The TMD 2D materials, especially $PdSe_2$ and PdS_2, have unique anisotropy structures, which enable the properties of these materials to be sensitive to the different geometries. Second, it was reported in previous literatures that the geometry we choose to simulate is more stable than other geometries[40-41].

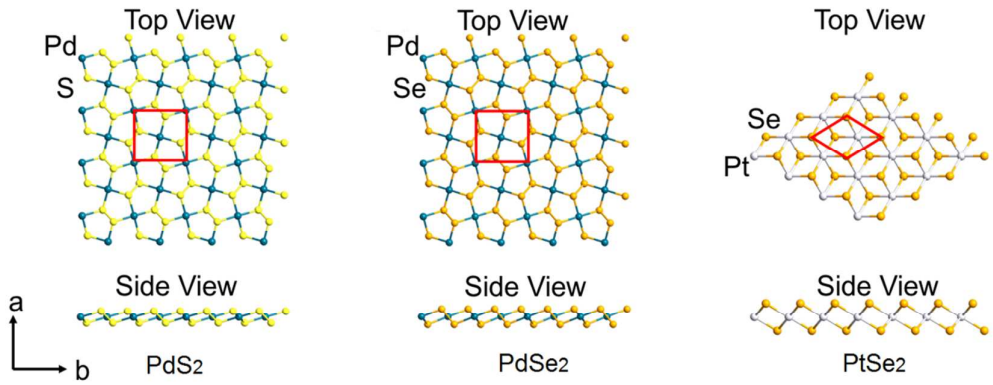

Figure 1. Schematic graphs of the 2D TW_2 type cells. The a and b lattice vectors are shown. The unit cells (red solid line) are indicated.

The band structures are calculated based on the density functional theory (DFT) with ATK software. The simulation configuration is similar to what was described in our previous work, with the key parameters such as mesh cut-off energy of 75 Hartree and 15×15×1 k-points grid used in the relaxation calculations. Shown in the Figure 2(a) and (b), we applied the asymmetrical biaxial strains along the a (ε_a) and b (ε_b) directions on the orthorhombic cell (PdS_2 and $PdSe_2$) and the symmetrical biaxial strains on the hexagonal cell ($PtSe_2$). The magnitude of deformation is defined as: $\Delta\varepsilon = (a - a_0)/a_0$, where a_0 and a are the lattice parameters of the unstrained and strained cells, respectively. Although it was stated that the PBE exchange correlation functional leads to a smaller value of the band gap, this paper focuses on the evolvement of the band structures of those monolayers under different strains. We mainly study the trend of the CBM, VBM and band gap change under mechanical strains of various magnitudes and directions. Therefore, how the strains affect the band structures change is the most important in this work. Moreover, it should not be a general statement to say the PBE method underestimates the band gap, which often depends on the material and system considered. Using the PBE exchange, we show that the band gap of monolayer PdS_2, $PdSe_2$ and $PtSe_2$ are 1.00 eV, 1.31 eV and 1.12 eV, which are very close to recent DFT calculations[28, 30, 42-43]. Hence it should be an appropriate option to use DFT-GGA for the Therefore, we believe that our choice of using the DFT-GGA (generalized gradient approximation) for the TW_2 materials.

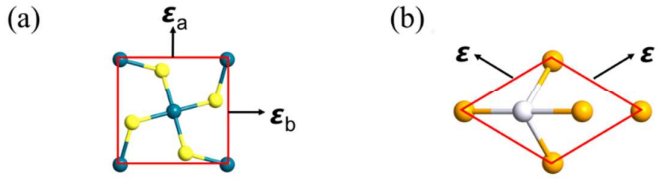

Figure 2. (a) Asymmetrical biaxial deformation along both a (ε_a) and b (ε_b) directions on the orthorhombic cell. (b) Symmetrical biaxial deformation ε on the hexagonal cell.

3 Simulation results and discussion

3.1 Electronic properties

We calculated band structures of the Brillouin zone of high symmetry points for various magnitudes of symmetrical biaxial strains along a and b directions on the monolayer PdS_2, $PdSe_2$ and $PtSe_2$ cells, as shown in Figure 3. The thick black lines in Figure 3 are the bands when zero strain is applied. The bands with various colors represent the bands under different strains. Figure 3(a) and (b) show the monolayer PdS_2 bands evolving with the applied compressive and tensile strains, respectively. In the strain-free state, the monolayer PdS_2 is indirect bandgap semiconductor with the conduction band minimum (CBM) and valence band maximum (VBM) at S and G point, respectively. Upon increasing the compressive strain (ε<0), the CBM increases and the VBM decreases. The CBM shifts from the S point to a point between Y and S under deformations from -4% to -10%. However, the VBM moves from the G point to a point between X and G under deformations from -2% to -10%. On contrast, increasing the tensile strains (ε>0), the CBM decreases and the VBM increases. Both the CBM and VBM are maintained at the S and G point. Eventually, the CBM and VBM cross the 0 eV for deformation of about 8%. Figure 3(c) and (d) show the monolayer $PdSe_2$ band evolving with the applied compressive and tensile strains, respectively. In the strain-free state, the monolayer $PdSe_2$ is an indirect band gap semiconductor with the CBM and VBM at a point between X and G. The CBM decreases and the VBM increases upon the compressive and tensile strains. The VBM is shifted from a point between X and G to a point between G and Y when the compressive deformation from -2% to -10%. However, under the tensile strains, The CBM is shifted from a point between X and G to the S point when the tensile deformation from 4% to 10%. While the VBM is shifted from a point between X and G to G point after 8% tensile deformation. Figure 3(e) and (f) show the monolayer $PtSe_2$ band evolving along symmetrical biaxial compressive and tensile strains, respectively. In strain-

free state, the monolayer $PtSe_2$ is an indirect band gap semiconductor with the CBM and VBM at a point between *G* and *M* and *G* point, respectively. Upon increasing the compressive strains, the VBM remains at the *G* point, while the CBM moves from a point between *G* and *M* to a point between *K* and *G* when the compressive deformation reaches -2%. Eventually, the CBM and VBM cross the 0 eV for compressive deformation of about -8%. However, under the tensile strains, the VBM moves from the *G* point to a point between *K* and *G* after 2% tensile deformation.

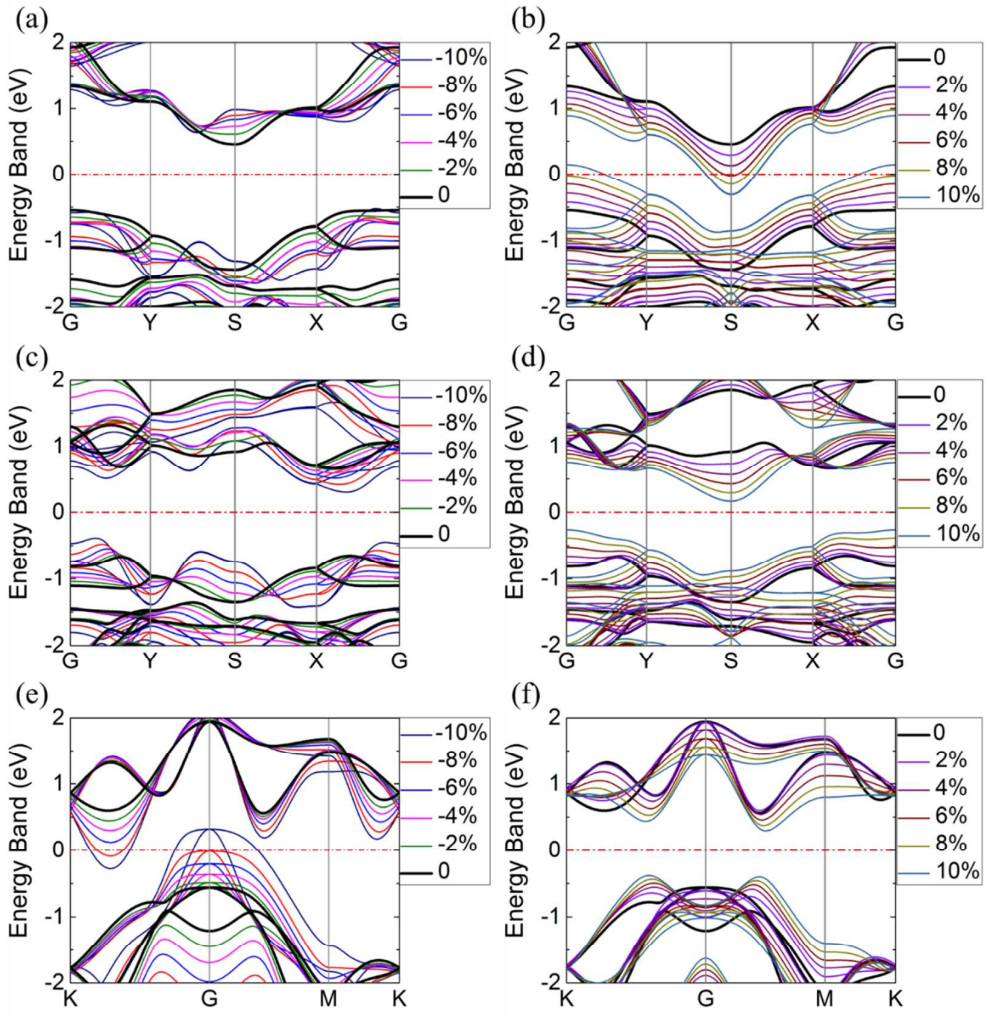

Figure 3. The band structures of the monolayer PdS_2 (a, b), $PdSe_2$ (c, d) and $PtSe_2$ (e, f) with symmetrical biaxial compressive and tensile strains.

The directional dependence on the strain induced CBM, VBM, and band gap variations of the orthorhombic cells has been studied according to the procedure described in our previous work[44]. Figure 4 and Figure 5 show the evolution of the CBM, VBM and band gap with the

biaxial strains along the both *a* and *b* directions on the monolayer PdS_2 and $PdSe_2$, respectively. Here, we only exhibit the CBM, VBM and band gap in the deformation with *a* and *b* ranging from 0 to 10%.

The calculated results of the CBM, VBM and bandgap of the PdS_2 for the compressive strains are shown in Figure 4(a, c and e). The common feature in these results is that it is not a monotonous change of the CBM, VBM and bandgap under the uniaxial compressive strains. Besides, we can also see that the minimum of the CBM occurs when no strain is applied and the maximum of the VBM is on the largest deformation with *a* and *b* directions. However, the maximum of the bandgap appears when the biaxial deformation is approximately 4% in *a* direction and 8% in *b* direction, which is different with the previous studies[34-35]. The difference in the strain values corresponding to the maximum bandgap from the reference[34] is due to that only tensile strains are considered in reference[34], however the strain values (4% in *a* direction and 8% in *b* direction) corresponding to the maximum of the bandgap in this work appear at compressive strains. Under the compressive strains, the reference[35] only considered the monolayer PdS_2 hexagonal cell under the symmetrical biaxial strains, which does not have the anisotropic property like orthorhombic cell (our paper), which leads to the difference in the strain values corresponding to the maximum of the bandgap. Figure 4(b, d and f) show the change of the CBM, VBM and bandgap for the tensile strains. The common feature in these results is the linear change for both *a* and *b* directions. The CBM and bandgap linearly decrease, while the VBM linearly increases. The minimum of the CBM is on the largest deformation state, while the maximum of the VBM and bandgap are on the largest deformation and the strain-free state respectively. Obviously, the symmetrical biaxial strains are more effective than the uniaxial strains in change the bandgap.

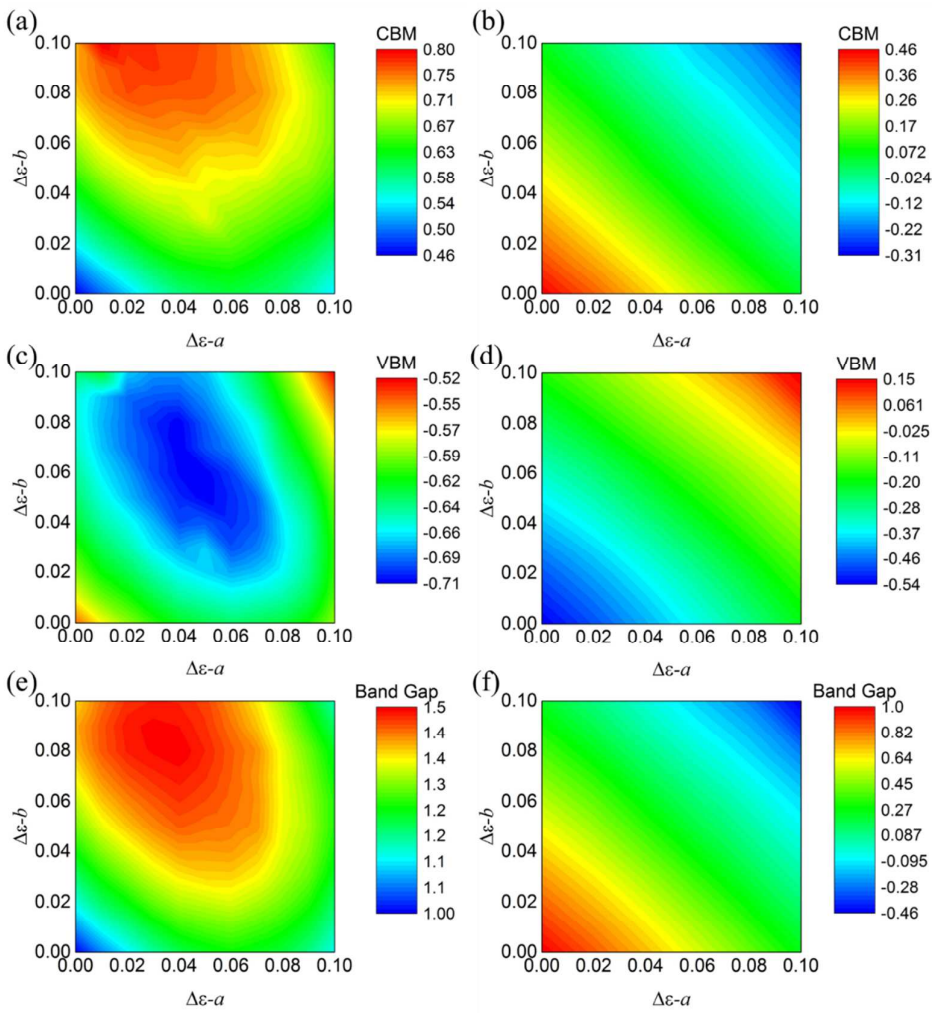

Figure 4. CBM, VBM and bandgap for the monolayer PdS_2 with compressive (a, c and e) and tensile (b, d and f) strains, respectively.

Figure 5 shows the changes of the CBM, VBM and bandgap for the monolayer $PdSe_2$ under different strains. The common aspect in these results is that a monotonous change for strains in *a* and *b* directions. The CBM and bandgap decrease with increasing strains, while the VBM increases. The minimum of the CBM is on the largest deformation, while the maximum of the VBM and bandgap are on the largest deformation and strain-free state respectively. The changes of the CBM, VBM and bandgap under uniaxial *a* or *b* direction strains is weaker than symmetrical biaxial strains.

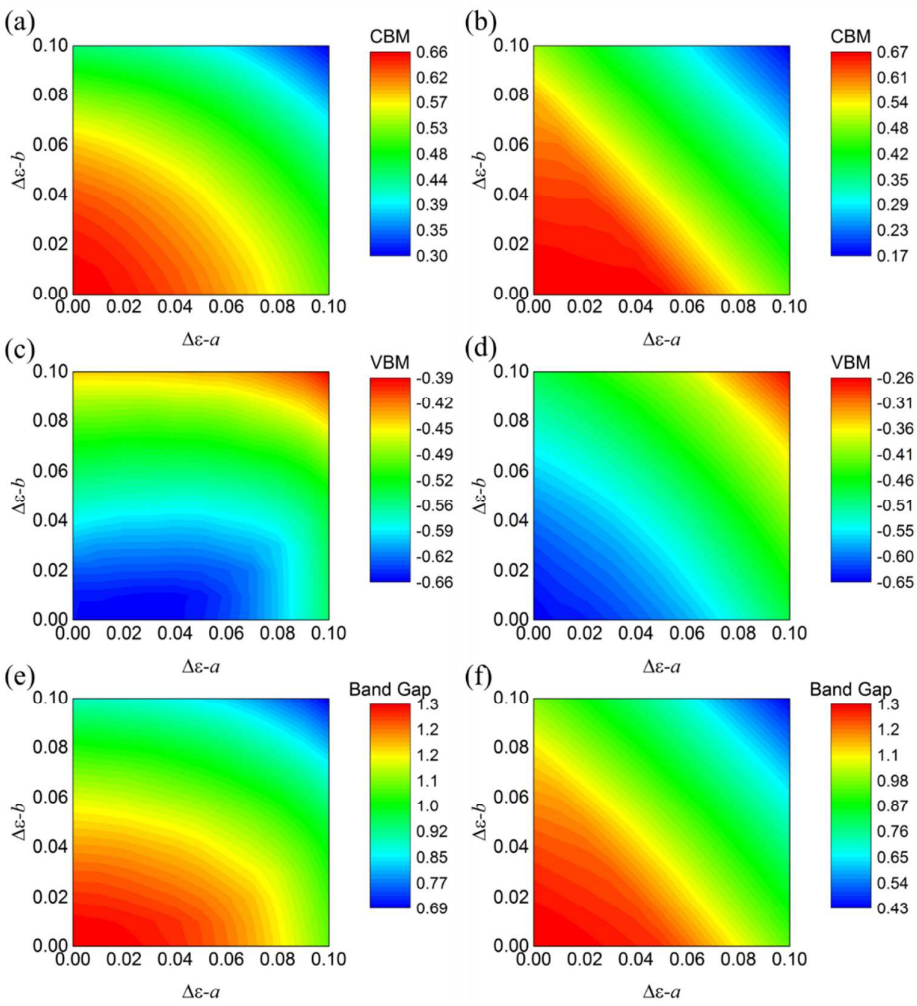

Figure 5. CBM, VBM and bandgap for the monolayer $PdSe_2$ with compressive (a, c and e) and tensile (b, d and f) strains, respectively.

In the following, we analyze the impact of biaxial symmetrical strains on the monolayer $PtSe_2$, and results are in Figure 6. It shows that the CBM and bandgap firstly increase and then decrease from compressive to tensile deformations. However, the change of the VBM is the opposite to that of the CBM and bandgap. The extreme points of the CBM, VBM and bandgap are at about 2% tensile deformation, which is a good agreement with previously reported results[30, 33]. Among these three materials, PdS_2 exhibits excellent electronic tunability under tensile strains because it displays a steady evolution of the CBM, VBM and bandgap under tensile strains (Figures 4b, 4d and 4f).

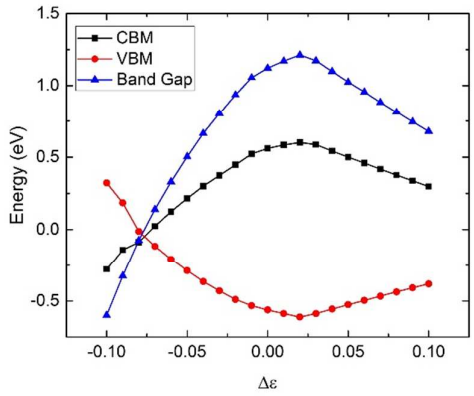

Figure 6. CBM, VBM and bandgap for the monolayer $PdSe_2$ under the biaxial symmetrical strains.

To gain more physical insights on the evolution of band structures of monolayer TW_2 with strains, the bands of monolayer TW_2 is resolved for the *d*, *p* and *s* orbitals in Figure 7. The conduction band minimum (CBM) and valence band maximum (VBM) have the contribution mainly from the *d* and *p* orbitals. The VBM is mainly contributed by the p_z and p_y orbital of *X* atom, while the CBM is mainly contributed by *M* (d_{xy} & d_{zy}) and *X* (p_z & p_y). These different of orbitals coupling lead to the VBM and CBM exhibit different response behaviors to external strain [34, 35]. The common feature in these materials is that the *d* and *p* orbital coupling is primarily composed the bands near the Fermi energy. The bandgap is determined by the *d* and *p* orbital coupling. Application of compressive strain increases the *d* and *p* orbital coupling. While the coupling between the *d* and *p* orbital is weaker under the tensile strain. Figure 7(b), (e) and (h) show the PDOS of the monolayer PdS_2, $PdSe_2$ and $PtSe_2$ under the strain-free state. Under the compressive strains (Figure 7(a), (d) and (g)), the stronger *d* and *p* orbital coupling near the VBM for PdS_2 and $PdSe_2$, near the CBM for PdS_2 and $PtSe_2$. However, under the tensile strains (Figure 7(c), (f) and (i)), the *d* and *p* orbital coupling becomes weaker near VBM and CBM of the monolayer PdS_2, $PdSe_2$ and $PtSe_2$. The above results signify that the mechanical strain plays a distinct role for band structures and modulate the electrical property of the monolayer PdS_2, $PdSe_2$ and $PtSe_2$.

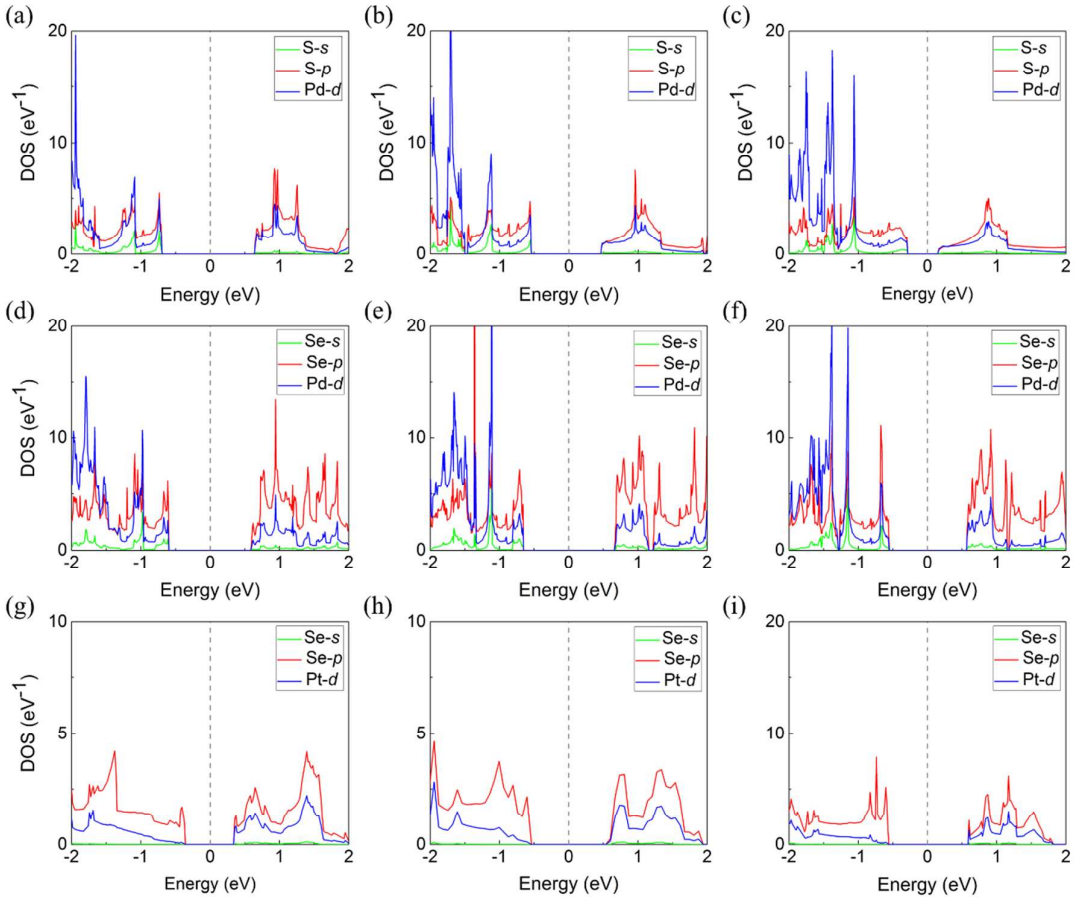

Figure 7. The PDOS of the monolayer PdS_2 (a)-(c), $PdSe_2$ (d)-(f), and $PtSe_2$ (g)-(i) under the symmetrical biaxial strains of -4% (a, d, and g), 0 (b, e and h) and 4% (c, f and i).

3.2 Mechanical properties

Shown in Figure 8, the spatial distribution of the charge density for the single layer PdS_2, $PdSe_2$ and $PtSe_2$ unit cells at the zero strain has been simulated with the DFT software and the results are displayed. The figure shows the bonding structure of the materials, where the bonding force is the function of atomic distance and the bonding angle between adjacent atoms. The underlying relation between the mechanical property – Young's modulus and the atomic bonding characteristics can be found in our previous work[9].

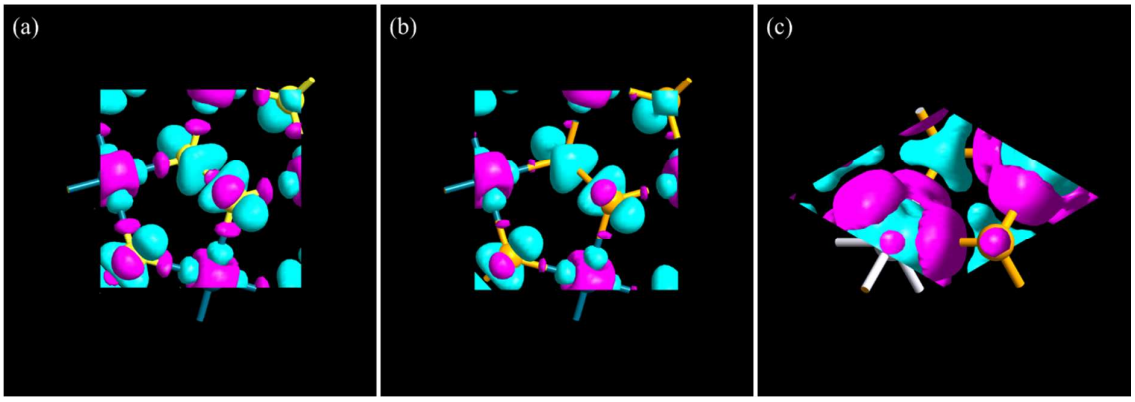

Figure 8. Partial charge density of monolayer PdS_2 (a), $PdSe_2$ (b) and $PtSe_2$ (c) unit cells. The isosurface value was taken as 0.05 $e/Å^3$.

Young's modulus of all three materials (Y_{PdS2}, Y_{PdSe2}, and Y_{PtSe2}) can be calculated using the *ab initio* methods in the *a* and *b* direction[25]. We used strain-stress method to calculate the Young's modulus and have taken the value in a very small range of strain values, as the strain-stress relation can be assumed to be linear in small deformations. According to the mechanical theory[45], linear strain-stress relation is exhibited in the small deformation (strain) range. The linear relation indicates that the material is operated in the elastic region and that the monolayer PdS_2, $PdSe_2$ and $PtSe_2$ are very ductile materials. Large deformation causes nonlinearity of the strain-stress relation and ultra-large deformation sometimes leads to plastic deformation or fracture. We can obtain the corresponding elastic modulus from the linear region to the stress-strain curve. In the strain-stress method, the stress (σ) and strain (ε) tensors are always symmetric 3×3 matrices, and they can be written in the form of 6-vectors, using the Voigt natation[46]:

$$\sigma = (\sigma_{xx}, \sigma_{yy}, \sigma_{zz}, \sigma_{yz}, \sigma_{xz}, \sigma_{xy}) \quad (1)$$

$$\varepsilon = (\varepsilon_{xx}, \varepsilon_{yy}, \varepsilon_{zz}, 2\varepsilon_{yz}, 2\varepsilon_{xz}, 2\varepsilon_{xy}) \quad (2)$$

The linear response of the stress vector to a given strain vector can then be written as:

$$\sigma = C \cdot \varepsilon \quad (3)$$

where the symmetric 6×6 matrix *C* contains the elastic constants:

$$C = \begin{pmatrix} C_{11} & C_{12} & C_{12} & 0 & 0 & 0 \\ C_{12} & C_{11} & C_{12} & 0 & 0 & 0 \\ C_{12} & C_{12} & C_{11} & 0 & 0 & 0 \\ 0 & 0 & 0 & C_{44} & 0 & 0 \\ 0 & 0 & 0 & 0 & C_{44} & 0 \\ 0 & 0 & 0 & 0 & 0 & C_{44} \end{pmatrix} \quad (4)$$

To obtain the elastic constants, one should apply small deformation to the simulated cell along selected strain vectors and calculate the resulting stress vectors. The Young's modulus (Y) can then be calculated by:

$$Y = \frac{C'_{11} - C_{11}}{\Delta\varepsilon} \quad (5)$$

Under large deformations, mechanical nonlinearity causes significant change of the Young's modulus (result will be much smaller if the material exhibits spring softening effect in large strain values). Calculated results in Figure 9 shows that the stress-strain curve first of all demonstrates a nonlinear performance, meaning the Young's modulus has a slightly reducing trend, representing the material softening property. In Figure 9, stress-strain curve shows a linear trend in a small strain region (linear region), the Young's modulus for three materials are calculated and shown in Figure 9. It shows Y_{PdS2}>Y_{PtSe2}>Y_{PdSe2} along the a direction and Y_{PdS2}>Y_{PdSe2}>Y_{PtSe2} along the b direction. We calculated a wider range stress-strain relation for obtaining the Young's modulus in Figure. S1(in the Supporting Information). As the applied strain increases ($|\Delta\varepsilon| > 10\%$), the calculated stress-strain behaviors become nonlinear and fluctuation. Based on the calculated stress-strain curve along, it appears that the monolayer TW_2 are more stable under the tensile strains when the strain is within 10%. Comparing the Young's modulus of PdS_2 in this work and reference[34], the results have significant difference, which because that we used strain-stress method to calculate the Young's modulus and conducted the calculation in a very small range of strain values, as the strain-stress relation can be assumed to be linear in small deformations. Under large deformations, mechanical nonlinearity causes significant change of the Young's modulus (result will be much smaller if the material exhibits spring softening effect in large strain values).

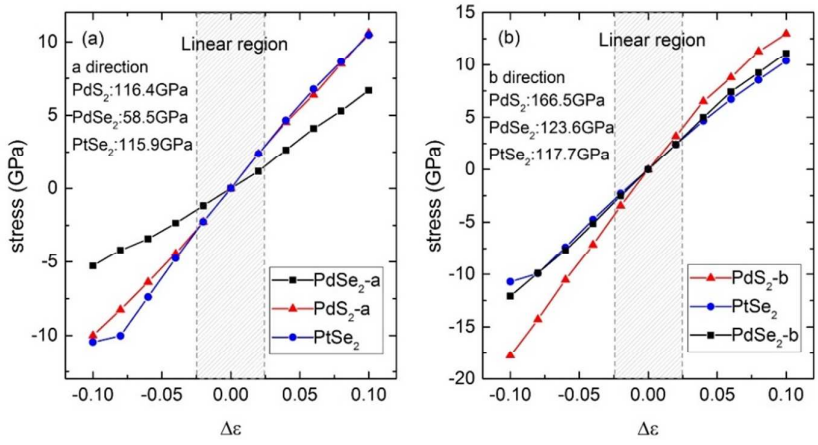

Figure 9. The strain-stress relation of monolayer PdS_2, $PdSe_2$ and $PtSe_2$ in the a (a) and b (b) direction.

3.3 Optical properties

The change of bandgap affects the optoelectronic properties of the monolayer PdS_2, $PdSe_2$ and $PtSe_2$. We calculated the optical properties of these materials under the biaxial strains. By using the Kubo-Greenwood formula, the susceptibility tensor has the form as[46]:

$$\chi_{ij}(\omega) = -\frac{e^2\hbar^4}{m^2\epsilon_0 V\omega^2}\sum_{nm}\frac{f(E_m)-f(E_n)}{E_{nm}-\hbar\omega-i\Gamma}\pi^i_{nm}\pi^j_{mn} \quad (6)$$

where e, $\hbar$ and ϵ_0 are the elementary charge, reduced Planck constant and vacuum dielectric constant. π^i_{nm} is the i-th component of the dipole matrix element between state n and m. E_m, E_n and E_{nm} are the energy level at m, n and between state n and m. V, Γ and f are the volume, broadening and Fermi function, respectively. The relative dielectric constant (ϵ_r) are related to the susceptibility as:

$$\epsilon_r(\omega) = (1 + \chi(\omega)) \quad (7)$$

The ϵ_1 and ϵ_2 are the real and imaginary parts of the complex dielectric constant. Figure shows the simulated ϵ_1 and ϵ_2 spectrums versus energy for various strains on the monolayer PdS_2, $PdSe_2$ and $PtSe_2$. The bold black lines in Figure 10 are the spectrums without strain. In general trend, the peak of the complex dielectric constant red-shifts (longer wavelength) towards lower energy with increasing compressive and tensile strains. To understand the origin of the red-shift of the above optical characteristics, we take a close look at the strain-dependent band structures for various strain values in Figure 3. Upon increasing the tensile strain, the CBM decreases and VBM increases. With the decrease of the band gap of the monolayer TW_2, the peak wavelengths of the ϵ_1 and ϵ_2 reduce (red-shifted). Moreover, it is clear from the Figure 10 that the real part of the static dielectric constant $\epsilon_1(0)$ (points at 0 of the energy axis) have certain values, and then it increases when the absolute value of the strain increases for all materials. This trend is opposite to the evolution of the bandgap because the framework of Penn's model expression for semiconductors[33], $\epsilon_1(0) \approx 1 + (\hbar\omega_p/E_g)^2$ in which static dielectric constant is inversely proportional to the band gap. It is clear that strain is an effective method to modulate the optical properties of the monolayer PdS_2, $PdSe_2$ and $PtSe_2$. The results explicitly show that PdS2 is the best material for tunability, as it displays a steady shift from higher energy to lower energy under tensile strains (Figures 10a and 10b).

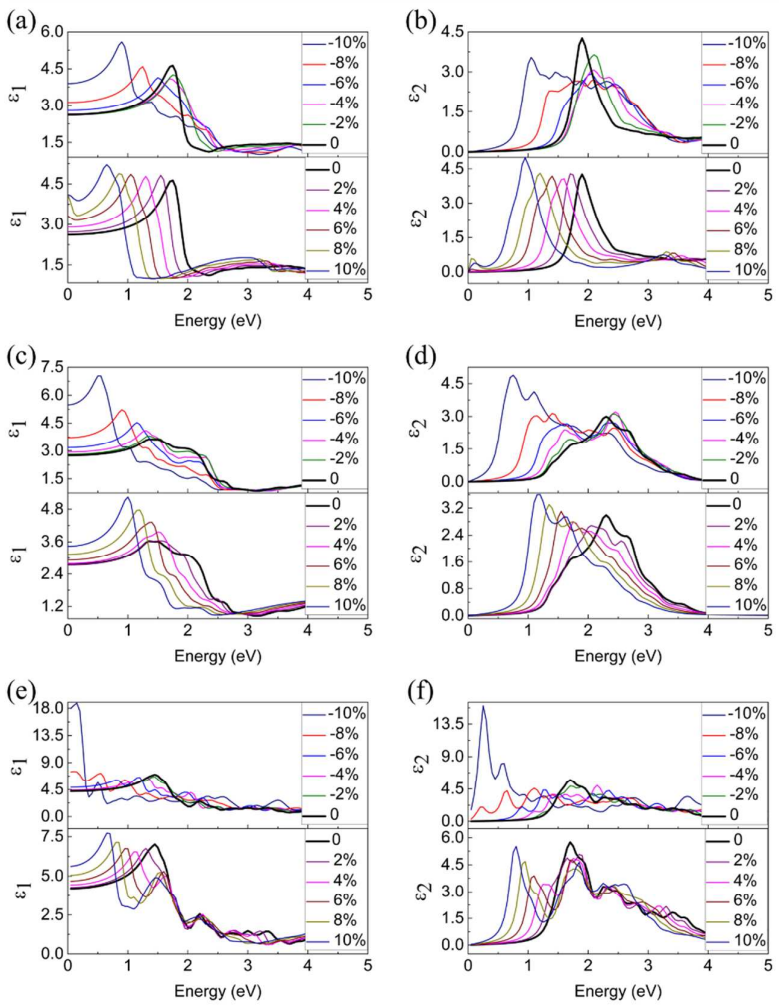

Figure 10. The real (ϵ_1) and imaginary (ϵ_2) parts of the complex dielectric constant of the monolayer PdS_2 (a, b), $PdSe_2$ (c, d) and $PtSe_2$ (e, f) under applied biaxial strains.

4 Conclusion

In this paper, the first-principles method has been used to study the band structures, Young's modulus and complex dielectric constant of the monolayer PdS_2, $PdSe_2$ and $PtSe_2$. Hexagonal and orthorhombic cells of three materials have been constructed and calculated when a mechanical strain is applied, which varies in both the direction and magnitude. It is revealed that these materials especially PdS_2 and $PdSe_2$ have unique anisotropy structures (Figure. S2 and S3 in the Supporting Information). The biaxial strains affect the band structure properties more significantly than the uniaxial strains. In the stress-strain study, it has been simulated that the Young's modulus of these three materials has the relation of $Y_{PdS2}>Y_{PtSe2}>Y_{PdSe2}$ along the *a* direction and $Y_{PdS2}>Y_{PdSe2}>Y_{PtSe2}$ along the *b* direction. For the optical properties, the

peaks of the real and imaginary parts of the complex dielectric constant red-shift towards lower energy; and $\epsilon_1(0)$ monotonously increases with the increasing compressive and tensile strains. Comparing the strain tunable electronic and optical properties, the monolayer PdS_2 exhibits excellent electronic and optical tunability from 0 to 10% tensile deformation. First, upon applying the tensile strains, the bandgap of the monolayer PdS_2 decreases approximately linearly (Figures 2b, 2d, 2f) and the strain tunability are -0.07 eV, -0.08 eV and -0.14 eV for 1% deformation with uniaxial *a*, *b* and symmetrical biaxial tensile strains. Second, the peak of dielectric constant curve demonstrates a stable red-shift (Figures 10a, 10b) under the symmetrical biaxial tensile strains. The strain tunability are -0.11 eV and -0.09 eV for 1% deformation with real and imaginary parts of the complex dielectric constant. The monolayer PdS_2 excellent electronic and optical tunability make it a compelling candidate for high sensitivity optical sensors.

5 Acknowledgements

Authors are grateful for funding by the China Scholarship Council (CSC).

ASSOCIATED CONTENT

Supporting Information available:

Detailed descriptions of the lattice parameters and the piezoelectric tensor of the monolayer PdS_2, $PdSe_2$ and $PtSe_2$, the strain-stress relation in the *a* and *b* direction over a large range of strain values and the anisotropy properties of these materials.

AUTHOR INFORMATION

Corresponding Authors

Lijie Li, *email: L.Li@swansea.ac.uk

Yan Zhang, *email: zhangyan@uestc.edu.cn

Notes

The authors declare no competing financial interest.

References

(1) Li, L. J.; Zhang, Y. Controlling the Luminescence of Monolayer MoS2 Based on the Piezoelectric Effect. *Nano Research* **2017**, *10,* 2527-2534.
(2) Surrente, A.; Dumcenco, D.; Yang, Z.; Kuc, A.; Jing, Y.; Heine, T.; Kung, Y. C.; Maude, D. K.; Kis, A.; Plochocka, P. Defect Healing and Charge Transfer-Mediated Valley Polarization in MoS2/MoSe2/MoS2 Trilayer Van Der Waals Heterostructures. *Nano Letters* **2017**, *17,* 4130-4136.
(3) Park, K. D.; Khatib, O.; Kravtsov, V.; Clark, G.; Xu, X. D.; Raschke, M. B. Hybrid Tip-Enhanced Nanospectroscopy and Nanoimaging of Monolayer WSe2 with Local Strain Control. *Nano Letters* **2016**, *16,* 2621-2627.
(4) Addou, R.; McDonnell, S.; Barrera, D.; Guo, Z. B.; Azcatl, A.; Wang, J.; Zhu, H.; Hinkle, C. L.; Quevedo-Lopez, M.; Alshareef, H. N.; Colombo, L.; Hsu, J. W. P.; Wallace, R. M. Impurities and Electronic Property Variations of Natural MoS2 Crystal Surfaces. *ACS Nano* **2015**, *9,* 9124-9133.
(5) Fu, X. P.; Li, F. F.; Lin, J. F.; Gong, Y. B.; Huang, X. L.; Huang, Y. P.; Han, B.; Zhou, Q.; Cui, T. Pressure-Dependent Light Emission of Charged and Neutral Excitons in Monolayer MoSe2. *J Phys Chem Lett* **2017**, *8,* 3556-3563.
(6) Castellanos-Gomez, A.; van Leeuwen, R.; Buscema, M.; van der Zant, H. S. J.; Steele, G. A.; Venstra, W. J. Single-Layer MoS2 Mechanical Resonators. *Adv. Mater.* **2013**, *25,* 6719-6723.
(7) McKenna, A. J.; Eliason, J. K.; Flannigan, D. J. Spatiotemporal Evolution of Coherent Elastic Strain Waves in a Single MoS2 Flake. *Nano Lett.* **2017**, *17,* 3952-3958.
(8) Yu, Z. H.; Pan, Y. M.; Shen, Y. T.; Wang, Z. L.; Ong, Z. Y.; Xu, T.; Xin, R.; Pan, L. J.; Wang, B. G.; Sun, L. T.; Wang, J. L.; Zhang, G.; Zhang, Y. W.; Shi, Y.; Wang, X. R. Towards Intrinsic Charge Transport in Monolayer Molybdenum Disulfide by Defect and Interface Engineering. *Nature Communications* **2014**, *5*.
(9) Shuo, D.; Li, L. J.; Zhang, Y.; Li, M. Stability of Direct Band Gap under Mechanical Strains for Monolayer MoS2, MoSe2, WS2 and WSe2. *Physica E* **2018**, *101,* 44-49.
(10) Mak, K. F.; Lee, C.; Hone, J.; Shan, J.; Heinz, T. F. Atomically Thin MoS2: A New Direct-Gap Semiconductor. *Phys. Rev. Lett.* **2010**, *105,* 136805.
(11) Gutierrez, H. R.; Perea-Lopez, N.; Elias, A. L.; Berkdemir, A.; Wang, B.; Lv, R.; Lopez-Urias, F.; Crespi, V. H.; Terrones, H.; Terrones, M. Extraordinary Room-Temperature Photoluminescence in Triangular WS2 Monolayers. *Nano Letters* **2013**, *13,* 3447-3454.
(12) Chang, C. H.; Fan, X. F.; Lin, S. H.; Kuo, J. L. Orbital Analysis of Electronic Structure and Phonon Dispersion in MoS2, MoSe2, WS2, and WSe2 Monolayers under Strain. *Physical Review B* **2013**, *88,* 195420.
(13) Ross, J. S.; Wu, S. F.; Yu, H. Y.; Ghimire, N. J.; Jones, A. M.; Aivazian, G.; Yan, J. Q.; Mandrus, D. G.; Xiao, D.; Yao, W.; Xu, X. D. Electrical Control of Neutral and Charged Excitons in a Monolayer Semiconductor. *Nature Communications* **2013**, *4*.
(14) Ramasubramaniam, A. Large Excitonic Effects in Monolayers of Molybdenum and Tungsten Dichalcogenides. *Phys. Rev. B* **2012**, *86,* 115409.
(15) Cheiwchanchamnangij, T.; Lambrecht, W. R. L. Quasiparticle Band Structure Calculation of Monolayer, Bilayer, and Bulk MoS2. *Phys. Rev. B* **2012**, *85,* 205302
(16) Wu, S. F.; Ross, J. S.; Liu, G. B.; Aivazian, G.; Jones, A.; Fei, Z. Y.; Zhu, W. G.; Xiao, D.; Yao, W.; Cobden, D.; Xu, X. D. Electrical Tuning of Valley Magnetic Moment through Symmetry Control in Bilayer MoS2. *Nature Physics* **2013**, *9,* 149-153.
(17) Sallen, G.; Bouet, L.; Marie, X.; Wang, G.; Zhu, C. R.; Han, W. P.; Lu, Y.; Tan, P. H.; Amand, T.; Liu, B. L.; Urbaszek, B. Robust Optical Emission Polarization in MoS2 Monolayers through

Selective Valley Excitation. *Phys. Rev. B* **2014**, *89,* 079903.
(18) Zeng, H. L.; Dai, J. F.; Yao, W.; Xiao, D.; Cui, X. D. Valley Polarization in MoS2 Monolayers by Optical Pumping. *Nature Nanotechnology* **2012**, *7,* 490-493.
(19) Cao, T.; Wang, G.; Han, W. P.; Ye, H. Q.; Zhu, C. R.; Shi, J. R.; Niu, Q.; Tan, P. H.; Wang, E.; Liu, B. L.; Feng, J. Valley-Selective Circular Dichroism of Monolayer Molybdenum Disulphide. *Nature Communications* **2012**, *3*.
(20) Yu, F. F.; Liu, Q. W.; Gan, X.; Hu, M. X.; Zhang, T. Y.; Li, C.; Kang, F. Y.; Terrones, M.; Lv, R. T. Ultrasensitive Pressure Detection of Few-Layer MoS2. *Adv. Mater.* **2017**, *29*.
(21) Chang, Y. H.; Zhang, W.; Zhu, Y.; Han, Y.; Pu, J.; Chang, J. K.; Hsu, W. T.; Huang, J. K.; Hsu, C. L.; Chiu, M. H.; Takenobu, T.; Li, H.; Wu, C. I.; Chang, W. H.; Wee, A. T. S.; Li, L. J. Monolayer MoSe2 Grown by Chemical Vapor Deposition for Fast Photodetection. *ACS Nano* **2014**, *8,* 8582-8590.
(22) Mak, K. F.; McGill, K. L.; Park, J.; McEuen, P. L. The Valley Hall Effect in MoS2 Transistors. *Science* **2014**, *344,* 1489-1492.
(23) Fu, L.; Wan, Y.; Tang, N.; Ding, Y. M.; Gao, J.; Yu, J. C.; Guan, H. M.; Zhang, K.; Wang, W. Y.; Zhang, C. F.; Shi, J. J.; Wu, X.; Shi, S. F.; Ge, W. K.; Dai, L.; Shen, B. K-Lambda Crossover Transition in the Conduction Band of Monolayer MoS2 under Hydrostatic Pressure. *Sci Adv* **2017**, *3*.
(24) Sensoy, M. G.; Vinichenko, D.; Chen, W.; Friend, C. M.; Kaxiras, E. Strain Effects on the Behavior of Isolated and Paired Sulfur Vacancy Defects in Monolayer MoS2. *Phys. Rev. B* **2017**, *95,* 014106.
(25) Ghorbani-Asl, M.; Borini, S.; Kuc, A.; Heine, T. Strain-Dependent Modulation of Conductivity in Single-Layer Transition-Metal Dichalcogenides. *Physical Review B* **2013**, *87,* 235434.
(26) Scalise, E.; Houssa, M.; Pourtois, G.; Afanas'ev, V. V.; Stesmans, A. Strain-Induced Semiconductor to Metal Transition in the Two-Dimensional Honeycomb Structure of MoS2. *Nano Research* **2012**, *5,* 43-48.
(27) Wang, Y. L.; Li, L. F.; Yao, W.; Song, S. R.; Sun, J. T.; Pan, J. B.; Ren, X.; Li, C.; Okunishi, E.; Wang, Y. Q.; Wang, E. Y.; Shao, Y.; Zhang, Y. Y.; Yang, H. T.; Schwier, E. F.; Iwasawa, H.; Shimada, K.; Taniguchi, M.; Cheng, Z. H.; Zhou, S. Y.; Du, S. X.; Pennycook, S. J.; Pantelides, S. T.; Gao, H. J. Monolayer PtSe2, a New Semiconducting Transition-Metal-Dichalcogenide, Epitaxially Grown by Direct Selenization of Pt. *Nano Lett.* **2015**, *15,* 4013-4018.
(28) Oyedele, A. D.; Yang, S. Z.; Liang, L. B.; Puretzky, A. A.; Wang, K.; Zheng, J. J.; Yu, P.; Pudasaini, P. R.; Ghosh, A. W.; Liu, Z.; Rouleau, C. M.; Sumpter, B. G.; Chisholm, M. F.; Zhou, W.; Rack, P. D.; Geohegan, D. B.; Xiao, K. PdSe2: Pentagonal Two-Dimensional Layers with High Air Stability for Electronics. *J. Am. Chem. Soc.* **2017**, *139,* 14090-14097.
(29) Miro, P.; Ghorbani-Asl, M.; Heine, T. Two Dimensional Materials Beyond MoS2 : Noble-Transition-Metal Dichalcogenides. *Angew Chem Int Edit* **2014**, *53,* 3015-3018.
(30) Guo, S. D. Biaxial Strain Tuned Thermoelectric Properties in Monolayer PtSe2. *J. Mater. Chem. C* **2016**, *4,* 9366-9374.
(31) Zhao, Y. D.; Qiao, J. S.; Yu, Z. H.; Yu, P.; Xu, K.; Lau, S. P.; Zhou, W.; Liu, Z.; Wang, X. R.; Ji, W.; Chai, Y. High-Electron- Mobility and Air-Stable 2D Layered PtSe2 Fets. *Adv. Mater.* **2017**, *29*.
(32) ElGhazali, M. A.; Naumov, P. G.; Mirhosseini, H.; Suss, V.; Muchler, L.; Schnelle, W.; Felser, C.; Medvedev, S. A. Pressure-Induced Superconductivity up to 13.1 K in the Pyrite Phase of Palladium Diselenide PdSe2. *Phys. Rev. B* **2017**, *96,* 060509.
(33) Du, J.; Song, P.; Fang, L. Z.; Wang, T. X.; Wei, Z. M.; Li, J. B.; Xia, C. X. Elastic, Electronic

and Optical Properties of the Two-Dimensional PtX2 (X = S, Se, and Te) Monolayer. *Appl. Surf. Sci.* **2018**, *435,* 476-482.
(34) Wang, Y.; Li, Y. F.; Chen, Z. F. Not Your Familiar Two Dimensional Transition Metal Disulfide: Structural and Electronic Properties of the PdS2 Monolayer. *J. Mater. Chem. C* **2015**, *3,* 9603-9608.
(35) Ahmad, S. Strain Dependent Tuning Electronic Properties of Noble Metal Di Chalcogenides PdX2 (X = S, Se) Mono-Layer. *Mater. Chem. Phys.* **2017**, *198,* 162-166.
(36) Ahmad, S. Strained Noble Metal Di Chalcogenides PtX2 (X = S, Se) Mono-Layer: Ab Initio Study of Electronic and Lattice Dynamic Properties. *Physica E* **2018**, *95,* 139-143.
(37) Liu, X. B.; Zhou, H. C.; Yang, B.; Qu, Y. Y.; Zhao, M. W. Strain-Modulated Electronic Structure and Infrared Light Adsorption in Palladium Diselenide Monolayer. *Sci. Rep.* **2017**, *7*.
(38) Li, P. F.; Li, L.; Zeng, X. C. Tuning the Electronic Properties of Monolayer and Bilayer PtSe2 Via Strain Engineering. *J. Mater. Chem. C* **2016**, *4,* 3106-3112.
(39) Atomistix Toolkit (ATK), Https://Quantumwise.Com/. .
(40) Gronvold, F.; Haraldsen, H.; Kjekshus, A. On the Sulfides, Selenides and Tellurides of Platinum. *Acta Chem. Scand.* **1960**, *14,* 1879-1893.
(41) Gronvold, F.; Rost, E. The Crystal Structure of PdSe2 and PdS2. *Acta Crystallogr.* **1957**, *10,* 329-331.
(42) Sun, J. F.; Shi, H. L.; Siegrist, T.; Singh, D. J. Electronic, Transport, and Optical Properties of Bulk and Mono-Layer PdSe2. *Appl. Phys. Lett.* **2015**, *107*.
(43) Ghorbani-Asl, M.; Kuc, A.; Miro, P.; Heine, T. A Single-Material Logical Junction Based on 2D Crystal PdS2. *Adv. Mater.* **2016**, *28,* 853-856.
(44) Shuo, D.; Li, L. J.; Zhang, Y. Strain Magnitude and Direction Effect on the Energy Band Structure of Hexagonal and Orthorhombic Monolayer MoS2. *IEEE Trans. Nanotechnol* **2018**, 1-1.
(45) Gere, J. M. *Mechanics of Materials*, Thomoson Learning: 2004.
(46) Harrison, W. A. *Solid State Theory*, McGraw-Hill: 1970.

Strain Modulated Electronic, Mechanical and Optical Properties of the Monolayer PdS_2, $PdSe_2$, and $PtSe_2$ for Tunable Devices

Shuo Deng[†‡], Lijie Li*[‡], Yan Zhang*[¶]

[†]School of Logistic Engineering, Wuhan University of Technology, Wuhan 430070, China
[‡]College of Engineering, Swansea University, Swansea, SA1 8EN, United Kingdom
[¶]School of Physics, School of Physical Electronics, University of Electronic Science and Technology, Chengdu 610054, China

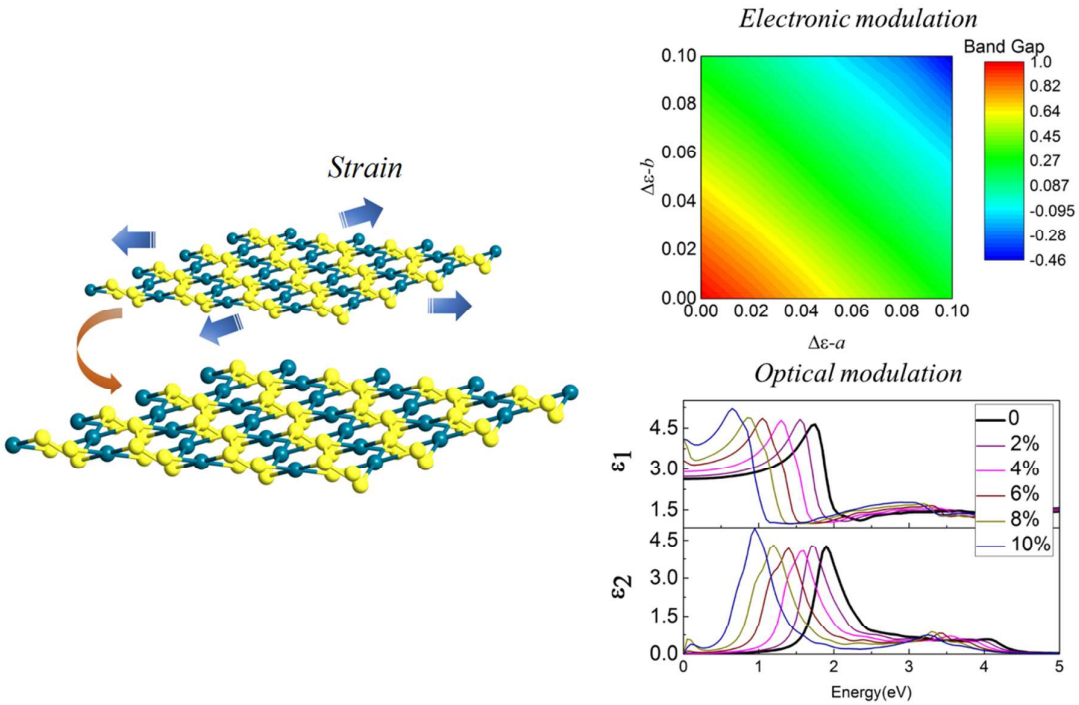

Table of content (TOC): From several group X TMD monolayer materials, PdS_2 has been found to exhibit linear electronic and optical response to the tensile strain effect.